Bioresource Technology Reports 18 (2022) 101010

Contents lists available at ScienceDirect

Bioresource Technology Reports

journal homepage: www.sciencedirect.com/journal/bioresource-technology-reports

Electro-cultivation of hydrogen-oxidizing bacteria to accumulate ammonium and carbon dioxide into protein-rich biomass

Narcís Pous [a,*], M. Dolors Balaguer [a], Silvio Matassa [b], Paola Chiluiza-Ramos [c], Lluis Bañeras [c], Sebastià Puig [a]

[a] Laboratory of Chemical and Environmental Engineering (LEQUiA), Institute of the Environment, University of Girona, Carrer Maria Aurèlia Capmany, 69, E-17003 Girona, Spain
[b] Department of Civil and Mechanical Engineering, University of Cassino and Southern Lazio, via G. di Biasio 43, 03043 Cassino, Italy
[c] Group of Molecular Microbial Ecology, Institute of Aquatic Ecology, University of Girona, C/Maria Aurèlia Capmany, 40, E-17003 Girona, Spain

ARTICLE INFO

Keywords:
Biocathode
Circular economy
Microbial Electrochemical Technologies
Resource recovery
Bioelectrochemical systems
Power-to-protein

ABSTRACT

Hydrogen-oxidizing bacteria (HOBs) are prime candidates for the sustainable production of microbial protein because of their high nutritional value and simple metabolic requirements, which could allow a simple resource recycling of NH_4^+ and CO_2 into a valuable product. The modality of hydrogen production/supply to HOBs represents a challenge. In this work, bioelectrochemical hydrogen and oxygen productions were coupled with HOBs cultivation in the same reactor. Using this approach, the protein content was 59 ± 8% with *Hydrogenophaga* and *Xanthobacter* as the most abundant HOBs. Biomass concentration was found to be dependent of the current density with bulk liquid biomass increasing between 101 and 124 mg TSS·L^{-1} for an increase of 0.1 mA·cm^{-2}. Electrodes directly immersed in the bioreactor promoted biofilm formation on the electrode surface, which could become an attractive alternative for biomass harvesting. The results of this work establish a novel proof-of-concept for bio-electro production of microbial protein.

1. Introduction

Nitrogen is an essential nutrient for life, being basically contained in proteins and nucleic acids. Current agro-systems are characterised by a low conversion efficiency of reactive nitrogen (fertilizers) into edible protein (4–14%) (Galloway and Cowling, 2002). Such low conversion efficiencies produce substantial environmental losses of reactive nitrogen, and result in severe externalities to both the environment and human health (Matassa et al., 2015a).

An innovative and resource-efficient alternative to produce protein could be found in microorganisms. Reactor-based cultivation of microbes enables the conversion of ammonium into protein at efficiencies (>90%) that are much higher than those of animal- or plant-based farming systems (31–47%) (Galloway and Cowling, 2002; Matassa et al., 2015a; Pikaar et al., 2017), and allows the synthesis of a final product characterized by protein contents as high as 70 to 80% (Matassa et al., 2020). Not only microbial protein (MP) production offers better ammonium assimilation efficiency, it implies also lower water and land footprints (Sillman et al., 2019). The widespread adoption of MP as an alternative nutritive source is dependent not only on the development of new methods to maximise their productivity and nutritional value, but also on finding strategies to gather the feedstocks needed (resource recovery). Taking all together, autotrophic microbial cultivation could be an appropriate choice. The selectivity of the growth medium used by autotrophic systems allows a better culture control without undermining the value of the final product (Matassa et al., 2015b; Volova and Barashkov, 2010). Carbon and nitrogen could be sourced from waste streams (e.g. flue gases and wastewater) in the form of CO_2 and ammonium (NH_4^+). This action could provide not only carbon and nitrogen sequestration, but also the upgrade into a valuable product: biomass. Among autotrophic microorganisms, hydrogen-oxidizing bacteria (HOBs) are gaining special attention. HOB can assimilate ammonium by using hydrogen as electron donor, carbon dioxide as a carbon source and oxygen (Eq. 1) or nitrate as electron acceptor (Matassa et al., 2016; Yu and Lu, 2019; Zhang et al., 2020) to produce a protein-rich biomass and also polyhydroxyalkanoates (PHAs) (Matassa et al., 2015b).

$$4H_2 + O_2 + CO_2 + 0.24NH_3 \rightarrow CH_{1.68}N_{0.24}O_{0.46} + 3.54H_2O \quad (1)$$

* Corresponding author.
E-mail address: narcis.pous@lequia.udg.cat (N. Pous).

https://doi.org/10.1016/j.biteb.2022.101010
Received 29 December 2021; Received in revised form 7 March 2022; Accepted 7 March 2022
Available online 12 March 2022

Being more complex to produce and manage than NH_4^+, O_2 or CO_2, techno-economically feasible hydrogen supply is crucial for HOB production. Over the last years the so-called hydrogen economy has gained momentum (De Vrieze et al., 2020; EU Hydrogen strategy, 2020), and hydrogen can now be obtained from a vast array of sources (Holladay et al., 2009; Hosseini and Wahid, 2016). Water electrolysis allows the direct production of H_2 from potentially renewable electricity, thereby improving the sustainability of the derived processes (Garcia-Garcia et al., 2020). Electricity-driven hydrogen production could be coupled to fermenters to cultivate HOBs and thus, to accumulate ammonium into protein-rich microorganisms (Christiaens et al., 2017; Matassa et al., 2016). How to couple water electrolysis and HOB cultivation is a challenge.

A two-steps process (an electrolyser to produce H_2 and a fermenter-like reactor to cultivate HOB) ensures a good control of the two units (Christiaens et al., 2017; Matassa et al., 2016). However, the need of sparging hydrogen into the bioreactor might presents limitations related to the low H_2 solubility (around 1.6 mg $H_2 \cdot L^{-1}$ at 1 atm and 298 K) and mass transfer rate.

The one-step process explores the in-situ production of H_2 and cultivation of HOB by electrodes immersion (Liu et al., 2016) or hydraulic connection (Givirovskiy et al., 2019; Ruuskanen et al., 2021). This method offers the advantage of improving the H_2 transfer while reducing the eventuality of generating explosive H_2/O_2 mixtures. However, the performances of one-step systems could be restrained by the need to find balance between the optimal conditions for H_2 generation and HOB cultivation (electrodes immersion), or be threatened by biomass clogging in case commercial electrolysers would be employed (hydraulic connection). Microbial Electrochemical Technologies (MET) has been demonstrated as an effective tool to promote the interaction between electrochemistry and bacteria. For example, they are an effective solution as biocatalyst for hydrogen evolution (Perona-Vico et al., 2020; Rozendal et al., 2008). This work develops a MET-based MP cultivation platform which explores the coupling of bio-electro-hydrogen production together with the cultivation of HOB. Both the structure and electrodes of the MET ensure a proper H_2 transfer and solubility for the HOB cultivation in the same reactor while reducing the risks of clogging for commercial electrolysers.

2. Materials and methods

2.1. Experimental set-up

Two reactors (Reactor A and B) were set-up and operated as replicates. Both reactors were assembled in three-neck bottles filled with 240 mL of liquid (150 mL of headspace). Both reactors presented a three-electrode configuration, with a cathode (working electrode), anode (counter electrode) and a reference electrode. The cathode electrode (working electrode) was stainless steel mesh (98 cm^2, mesh path light 5 × 5 mm). Stainless steel is a suitable metal for H_2 production (Kundu et al., 2013), and it ensures an easier biofilm removal compared to a porous carbon-based electrode. The anode (counter electrode) was a Ti covered with Mixed Metals Oxide (Ti-MMO) mesh (14 cm^2, NMT electrodes, South Africa) to promote O_2 evolution (Lai et al., 2017). An Ag/AgCl reference electrode was used (+0.197 V vs. SHE, SE 11, Xylem Analytics Germany Sales GmbH & Co. KG Sensortechnik Meinsberg, Germany). The system was operated under potentiostatic conditions, controlling the cathode potential at −0.997 V vs. Ag/AgCl using a potentiostat (Nanoelectra Nev3.2., Spain) and promoting biocathodic H_2 generation (Batlle-Vilanova et al., 2014). All tests were performed at 20 ± 2 °C.

2.2. Medium composition and reactor operation

The medium used to feed the two reactor replicates was modified from Matassa et al. (2016), by reducing the ammonium content and avoiding the vitamins addition. It contained 0.4 $g \cdot L^{-1}$ NH_4Cl (105 mgN-$NH_4^+ \cdot L^{-1}$), 1.05 $g \cdot L^{-1}$ $NaHCO_3$, 2.3 $g \cdot L^{-1}$ KH_2PO_4, 2.9 $g \cdot L^{-1}$ Na_2HPO_4, 0.5 $g \cdot L^{-1}$ $MgSO_4$, 0.01 $g \cdot L^{-1}$ $CaCl_2$ and 5 $mL \cdot L^{-1}$ micronutrients solution (Rabaey et al., 2005).

Both reactors were flushed twice a week with CO_2 for 10 min (99.9% Praxair, Spain) to simulate spent off-gases rich in CO_2.

Before starting the tests, a hydrogen-oxidizing enriched culture was developed in the laboratory from a denitrifying biocathode (Pous et al., 2017). Reactor's effluent was introduced in a 200 mL syringe bottle together with the medium described above and periodically flushed with H_2:CO_2 (20:80 *v*/v – Praxair, Spain) and air (21% O_2). Cultures were developed for >30 days with periodical replenishment of medium. When the HOB culture was developed, tests in the bioelectrochemical set-up started. Reactors were inoculated with an HOB culture as protein-rich biomass. Reactors were also inoculated with electroactive hydrogen-producing bacteria (Rovira-Alsina et al., 2020) to promote electricity-driven H_2 production at a lower energy cost (Batlle-Vilanova et al., 2014). A control test under Open Cell Voltage (OCV) conditions was run in a third single-cell reactor inoculated and operated following the same protocol.

2.3. Chemical analyses and calculations

Liquid samples were regularly taken from the bulk liquid to measure, conductivity and OD_{600} (DR3900, Hach Lange, Germany). The relationship between OD_{600} and total suspended solids (TSS) was evaluated experimentally (Eq. 2).

$$TSS = 1.31 \cdot OD_{600} \quad (2)$$

where, TSS are the total suspended solids (mg $TSS \cdot L^{-1}$), and OD600 is the optical density at 600 nm.

Total suspended solids (TSS), nitrite (N-NO_2^-), nitrate (N-NO_3^-), and ammonium (N-NH_4^+) were measured in accordance with the American Public Health Association (APHA) standards (APHA, 2005). In order to replace the extracted sampling volume, 60 mL were added every seven days (HRT of 28 days). At the end of the experimental period, electrodes were rinsed and washed biomass was analysed as total biomass. Biomass attached to the electrodes was calculated by subtracting the biomass analysed in the bulk liquid to the total biomass observed after electrode rinsing.

Gas samples were analysed periodically by gas chromatography (490 Micro GC system, Agilent Technologies, US) (Rovira-Alsina et al., 2020).

Proteins were quantified using a Quick Start™ Bradford 1× Dye Reagent (BioRad, USA) following the recommended instructions. Previously, cells partially disrupted using a beadbeater (MP instruments, 5 M/s, 30 s) and digested using alkaline conditions (1 M NaOH, 30 min at 95 °C). Digested cells were centrifuged to remove insoluble cell debris. All samples were diluted 1:10 to avoid interferences. Samples were analysed in triplicates.

Cyclic voltammetries (CVs) were recorded on the cathode electrode through a potential range from −1.2 to 0.0 V vs. Ag/AgCl. Three cycles were performed at scan rate 1 $mV \cdot s^{-1}$.

The maximum and average volumetric biomass productivity rate in the bulk liquid ($mgTSS \cdot L^{-1} \cdot d^{-1}$) and the related current density increase rate ($mA \cdot cm^{-2} \cdot d^{-1}$) was calculated from the linear regression of biomass concentration over time on days 0 to 13th in reactor A and days 27 to 60th in reactor B, respectively.

The average volumetric biomass extraction rate ($mgTSS \cdot L^{-1} \cdot d^{-1}$) was calculated by taking into account the total biomass extracted for sampling (mgTSS), the reactor volume (0.24 L) and the experimental time duration (60 days).

The average volumetric biofilm productivity rate on the cathode electrode surface was expressed per volume reactor ($mgTSS \cdot L^{-1} \cdot d^{-1}$) and calculated from the biomass rinsed from the biofilm ($mgTSS \cdot L^{-1}$) and the experimental time duration (60 days).

The ammonium removal rate ($mgN{\cdot}L^{-1}{\cdot}d^{-1}$) was calculated by dividing the ammonium removed ($mgN{\cdot}L^{-1}$) by the period of time evaluated (60 days). The overall nitrogen yield ($gTSS{\cdot}gN^{-1}$) was calculated by dividing the biomass produced ($mgTSS{\cdot}L^{-1}$) to the ammonium removed ($mgN{\cdot}L^{-1}$) along the experimental time duration (60 days).

Theoretical hydrogen production ($mgH_2{\cdot}L^{-1}$) was calculated from the current supplied (mA) during a specific period of time (days), considering the Faraday constant (96,485 mC·mmol e^{-1}), the moles required for H_2 formation (2 mol e^-·mole H_2^{-1}), the molecular weight (2 g·mole^{-1}) and the reactor volume (0.24 L). The hydrogen yield ($gTSS{\cdot}gH_2^{-1}$) was calculated by dividing biomass produced ($mgTSS{\cdot}L^{-1}$) and the estimated hydrogen produced ($mgH_2{\cdot}L^{-1}$) along the experimental time duration (60 days).

Theoretical oxygen production (mmole O_2) was calculated from the current supplied (mA) during a specific period of time (days), considering the Faraday constant (96,485 mC·mmole e^-) and the moles required for O_2 formation (4 mol e^-·mole O_2).

Power requirement (W) was calculated with the measured current (A) and cell voltage (V). Energetic requirements (Wh) were calculated by taking into account the power supplied (W) during an specific period of time (h). The energetic yield ($gTSS{\cdot}kWh^{-1}$) was calculated by taking into account the biomass produced (gTSS) and the energy dosed (kWh) along the experimental time duration (60 days).

2.4. Microbiological analyses

Biomass for DNA extraction was collected from the cathode stainless-steel mesh and bulk liquid of each reactor. Before DNA extraction, stainless-steel mesh was immersed in 4 mL of 0.1 M $Na_4P_2O_7{\cdot}10H_2O$ and treated in a sonication bath for 60 s (Selecta, Spain), followed by 30 s on ice. The suspended bacterial cells were centrifuged at 4000 rpm for 2 min (Vilajeliu-Pons et al., 2016). Samples from bulk liquid were centrifuged to collect cell pellets (4000 rpm, 10 min, 4 °C). DNA was extracted using the FastDNA® SPIN Kit for soil (MP, Biomedicals, Santa Ana, California, EUA), according to the manufacturer's instructions. The obtained DNA was quantified using a NanoDrop ND-1000 spectrophotometer (NanoDrop Technologies, Inc., Wilmington, DE) and stored at −20 °C. Illumina MiSeq flow cell (V2) sequencing was conducted by the RTSF Core facilities at the Michigan State University USA (https://rtsf.atsci.msu.edu/). The primers set 515F and 806R were used for the amplification of the V4 region of 16S rDNA (Kozich et al., 2013).

Sequences data from the MiSeq platform were quality filtered, trimmed, dereplicated, merged and, after a process of chimera removal, were clustered into amplicon sequence variants (ASVs) using the DADA2 Pipeline (Callahan et al., 2016). Afterwards, ASVs tabulation, chimera removal, and taxonomy assignment were performed using the Silva taxonomic database (v132). Finally, the Phyloseq package was used to tabulate relative abundances at various taxonomic levels (Nyyssölä et al., 2021). DADA2 was run as an R script (in R v.3.6.3) using R packages dada2 v.1.14.1, phyloseq v. 1.30.0. ASVs were assigned taxonomically using nucleotide Blast searches at NCBI.

3. Results and discussion

3.1. Electro-microbial protein production

Reactor replicates evolved during 60 days with an increase of microbial biomass from 60 to 182 ± 17 and 320 ± 54 $mgTSS{\cdot}L^{-1}$ in reactors A and B, respectively (mean data for days 40th to 60th) (Fig. 1). No biomass growth was observed in the reactor operated under OCV conditions (Supplementary Information). Along the whole duration of the experimental period, pH remained stable at 6.7 ± 0.3 and 6.7 ± 0.1, suggesting a proton (H^+) balanced process.

Despite the fact that reactors A and B were operated in a similar manner, their evolution over time differed when looking at point-to-point evolution. Reactor A showed an immediate activity, while reactor B presented some issues related to the potentiostat clamps during the first 10 days, which resulted in a fluctuating current (data not shown). Once these issues were solved, the stable operational phase started. In both reactors, suspended biomass concentration and current density showed a dependency. Reactor A presented an increase of current density together with an increase of biomass from day 0 to 13th. After day 13th, both biomass and current density remained mostly stable until the end of the experimental study. Reactor B presented a lag phase (days 10th to 27th) and a growth phase (days 27th to 60th), where both biomass and current density increased together. Steep variations in current density were related to CO_2 and medium replacement, and they are commonly observed in reactors where bio-electrochemical H_2 production is carried out (Rovira-Alsina et al., 2020).

A maximum volumetric biomass production rate of 17.0 and 61.4 $mgTSS{\cdot}L^{-1}{\cdot}day^{-1}$ and an average volumetric biomass production rate of 10.8 and 8.7 $mgTSS{\cdot}L^{-1}{\cdot}day^{-1}$ were observed for reactors A and B, respectively (Table 1). Current density increased at a rate of 0.011 and 0.007 $mA{\cdot}cm^{-2}{\cdot}day^{-1}$ in reactors A and B, respectively, during the growth phase periods. Considering the increase on current density together with the increase on biomass, it could be calculated that for an increase of 0.1 $mA{\cdot}cm^{-2}$, the suspended biomass concentration increased by 124 and 101 $mgTSS{\cdot}L^{-1}$, respectively. When the current density remained stable, the suspended biomass content remained stable as well (days 14th – 50th and 0 - 27th in reactors A and B, respectively). Under these stable phases, hydrogen was mainly used to replace the biomass extracted from the system (60 mL per week - biomass extraction rate of 3.6 and 3.4 $mgTSS{\cdot}L^{-1}{\cdot}day^{-1}$ for reactors A and B, respectively).

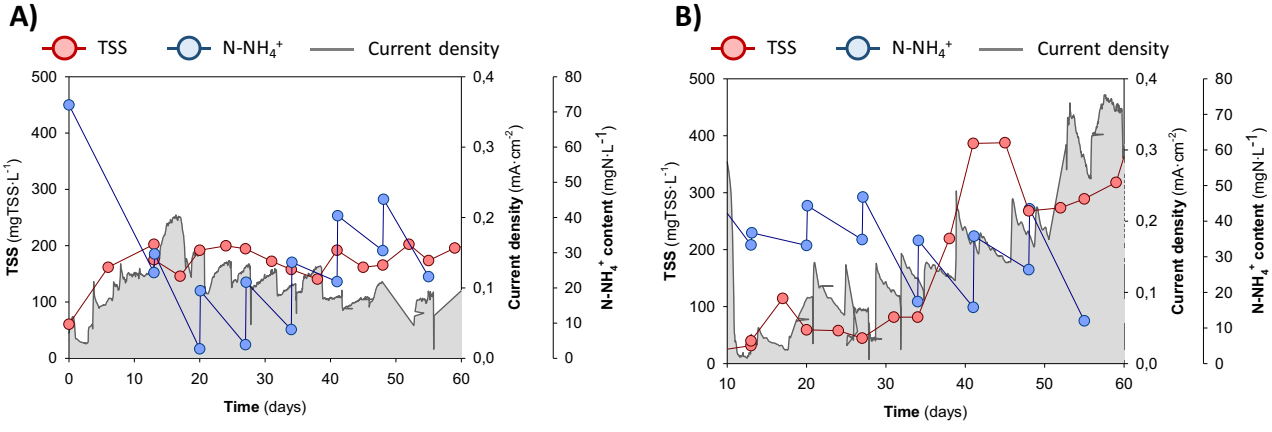

Fig. 1. Evolution of biomass (Total Suspended Solids, TSS), ammonium concentration and current density in reactor replicates A (A) and B (B).

Table 1
Summary of results obtained in this study compared with other works on hydrogen-oxidizing bacteria. Legend: BL = Bulk liquid (max: maximum; avg.: average); E = Electrode; TOT = Overall experimental period Electrode + Bulk liquid; SBR = Sequence Batch Reactor; CR = Continuous reactor; * = Hydrogen yields estimated by assuming that all current supplied to the cathode was converted into H_2, ** = Biomass data presented originally as cell dry weighHt (CDW), but assimilated here as TSS.

		Biomass production rate		Protein content	Hydrogen yield	Nitrogen yield	Microbial culture	Hydrogen and Oxygen source	Temperature
		(mg TSS·L^{-1}·d^{-1})	(mg TSS·mg TSS$_0^{-1}$·d^{-1})	(%)	(g TSS·g H$_2^{-1}$)	(g TSS·g N^{-1})		(H_2: O_2 ratio)	(°C)
Reactors of this study	A	17.0 (BL-max) 10.8 (BL-avg) 5.0 (E) 11.6 (TOT)	0.18	53 ± 8	0.29*	5.1	Mixed culture containing *Hydrogenophaga* sp. and *Xanthobacter* sp.	Produced in the reactor by BES (2: 1)	20 ± 2
	B	61.4 (BL-max) 8.7 (BL-avg) 3.8 (E) 12.6 (TOT)	0.15	64 ± 4	0.31*	5.5			
Matassa et al., 2016**		4488 ± 1080 (SBR) 9744 (CR)	9.0–15.0 (SBR) 19.5–32.5 (CR)	66 ± 5 (SBR) 71 ± 5 (CR)	1.28 ± 0.32 (SBR) 2.32 (CR)		Mixed culture dominated by *Sulfuricurvum* sp. (97%)	H_2 produced by electrolysis and sparged to the SBR. (3.25: 1)	28
Christiaens et al., 2017**		1720–1850	1.7–1.9		1.04–1.36			H_2 and O_2produced by electrolysis in two different cells and sparged to the reactor (3: 1)	23 ± 2
Givirovskiy et al., 2019		257					*Cupriavidis necator*	Bioreactor hydraulically connected to an electrolyser to provide H_2. Air sparging	30
Dou et al., 2019		264–288		63–64	1.0–1.1	0.3	*Paracoccus*	Sparged (3.5: 1)	30
Nyyssölä et al., 2021		238 ± 48	3.1 ± 0.6	36.9 ± 1.1	1.9 ± 0.4*		*N. nitrophenolicus*	Electrolysis in the reactor by with continuous CO_2: N_2 flush (2: 1)	30
		62 ± 19	0.7 ± 0.2	32.7 ± 1.7	0.5 ± 0.2*		*R. opacus*		

No harming of biomass related to high currents were expected at the tested current densities (<0.4 mA·cm^{-2}) (Zhang et al., 2020).

Along the whole experimental period biomass was analysed only in the bulk liquid, but cells attached to the electrodes were also observed as a thick biofilm only on the cathode electrode. This observation could be related to the fact the H_2 is the limiting substrate for HOB cultivation (Eq. 1). At the end of the study (day 60th), biomass loosely attached to the cathode was rinsed in the same reactor solution and analysed. These results showed a total biomass content (suspended biomass and biofilm) of 480 and 551 mgTSS·L^{-1} in reactors A and B, respectively. These values were higher than those observed in the bulk liquid alone (182 and 320 mgTSS·L^{-1}, respectively). If it is assumed that the biofilm was constantly growing along the whole duration of the experimental study, an average volumetric biofilm production rate of 5.0 and 3.8 mgTSS·L^{-1}·day^{-1} (12.2 and 9.4 mgTSS·cm^{-2}·day^{-1}) would be estimated for reactors A and B, respectively. Taking all data together (biofilm and bulk liquid), the average volumetric biomass production rate was estimated as 11.6 and 12.5 mgTSS·L^{-1}·day^{-1} for reactors A and B, respectively. It remains unclear whether biofilm evolved in a similar trend as the biomass in the bulk liquid and how were they affecting each other. According to the above discussed figures, biofilm growth accounted for about 43 and 31% of the overall final volumetric biomass productivity.

The volumetric production rates observed in this study were lower than those shown for systems where H_2 gas was sparged, which are the highest HOBs growth rates reported so far (Table 1). For example, HOB growth rate of 4488 ± 1080 mgTSS·L^{-1}·d^{-1} was observed in a sequencing batch reactor (SBR) or 9744 mgTSS·L^{-1}·d^{-1} when the reactor was operated in continuous-flow mode (Matassa et al., 2016). When combining ammonium recovery from urine with HOB cultivation in a bubble column, a volumetric biomass productivity rate of 1720–1850 mgTSS·L^{-1}·d^{-1} was shown (Christiaens et al., 2017). A single factor cannot explain the differences in productivity rates, but a combination of them. For example, the present study started with an inoculum presenting a biomass of 60 mgTSS·L^{-1}, while previous studies inoculated the reactor with concentrations of 77–91 mgTSS·L^{-1} (Nyyssölä et al., 2021), 300–500 mgTSS·L^{-1} (Matassa et al., 2016) or 1000 mgTSS·L^{-1} (Christiaens et al., 2017). If the inoculum concentrations are taken into account, the specific growth rate observed in reactors A and B was of 0.18 and 0.15 mg TSS·mgTSS$_0^{-1}$·d^{-1} (20 °C). While it has been observed rates between 0.7 and 3.1 mg TSS·mgTSS$_0^{-1}$·d^{-1} (30 °C) (Nyyssölä et al., 2021), or 19.5–32.5 mgTSS·mgTSS$_0^{-1}$·d^{-1} in continuous flow mode (28 °C) (Matassa et al., 2016). It is worth noting that the study presented here were performed at room temperature (20 ± 2 °C), while most of the works have been performed at higher temperatures (Dou et al., 2019; Givirovskiy et al., 2019; Matassa et al., 2016; Nyyssölä et al., 2021) (Table 1).

A relevant comparison is the work recently reported by Nyysölä and co-workers, where HOB pure cultures (*N. nitrophelicus* and *R. opacus*) were cultivated at 30 °C using a bioreactor with an immersed electrolyser (Nyyssölä et al., 2021). A maximum volumetric biomass production rate of 238 ± 48 and 62 ± 19 mg TSS·L^{-1}·day^{-1} for *N. nitrophelicus* and *R. opacus*, respectively, was observed. The differences on temperature (30 °C instead of the 20 °C) and the operation under a continuous CO_2:N_2 flow stream could explain the different growth rates observed.

Regarding the ammonium assimilation, protein analyses performed at the end of the study revealed a protein content of 53 ± 8% and 64 ± 4% in reactors A and B, respectively (Table 1). These values were higher than those reported by using an immersed electrolyser (32.7–36.9%) (Nyyssölä et al., 2021), but similar to the values observed by H_2 sparging in a sequence batch reactor (66 ± 5%) or a continuous reactor (71 ± 5%) (Matassa et al., 2016). If the total final balance in terms of nitrogen consumption and biomass production is considered, the calculated nitrogen yield was 5.1 and 5.5 gTSS·gN^{-1}, respectively. As a mean of comparison, the stoichiometric nitrogen yield for *Cupriavidis necator* is 7.3 gTSS·gN^{-1} (Yu and Lu, 2019). Hence, the values observed in this study were slightly lower than HOB stoichiometric values. It might indicate the presence of parallel nitrogen reactions inside the reactor (i.e. nitrification). Nitrate and nitrite were only detected at low concentrations along the experimental process (0.3 ± 2.7 mg N-NO_2^-·L^{-1} and 1.5 ± 2.0 mg N-NO_3^-·L^{-1}), suggesting that both nitrification and denitrification processes could be occurring in the reactor. In fact, when considering a crude protein content of 53–64% for the biomass

produced, as well as a nitrogen-to-protein ratio of 6.25, the calculated nitrogen biomass content would be 8.5–10.2% in the reactors. In addition, if all the consumed nitrogen, as measured through the nitrogen yield, would have been converted into biomass, the average N content of biomass would be 19.5 and 18.3% for reactors A and B, respectively. Based on these assumptions, the impact of the nitrification/denitrification process can be estimated to be around 56 and 44% of nitrogen removed, respectively.

Taking all together, the system presented here allowed electricity-driven ammonium accumulation in protein-rich bacteria. Bacteria were not only cultivated in the bulk liquid, but also as biofilm, which would allow a cheaper harvesting and dewatering of the product. Higher current densities allowed a higher biomass growth. Nevertheless, the system still requires optimization, both in terms of volumetric biomass productivities as well as in relation to the parallel, unwanted, nitrogen reactions. In order to better understand the processes occurring in the system, hydrogen and oxygen supply rates and ratios and the microbial community richness require special attention.

3.2. Hydrogen and oxygen supply efficiency

The volumetric biomass productivity in the electro-protein set-up depended on the current density. Higher current densities lead to a higher production of hydrogen (cathode) and oxygen (anode), providing the required substrates for biomass growth. At a poised cathode potential, the current density depends on the cathode activity. If an abiotic activity on the electrode is taking place, a pattern of stable current density would be expected. In the current study, the basal/abiotic cathode activity would be related to the current observed at the beginning of the experimental period (<0.10 $mA{\cdot}cm^{-2}$ in both reactors). As the MET reactors started to run, an evolution of current density was observed in both replicates, suggesting that an increase of activity was occurring on the cathode surface. Since the systems were inoculated electroactive hydrogen-producing bacteria (Rovira-Alsina et al., 2020), it was considered that the increase of cathode activity was related to the growth of H_2-producing bacteria. A piece of representative evidence was observed in the cyclic voltammetries (CVs) recorded in reactor B (Fig. 2). On day 7th, the current density at cathode potential values <−0.85 V vs. Ag/AgCl was around −0.1 $mA{\cdot}cm^{-2}$. On day 49th, the current density at this potential window had increased to −0.5 $mA{\cdot}cm^{-2}$. Considering that cathode potentials below −0.85 V vs. Ag/AgCl fit in the H_2 evolution zone, this result indicates that an increase of activity towards H_2 evolution occurred from day 7th to day 49th. Not only the current density increased, but also the onset potential (i.e. potential at which H_2 starts to be produced) moved from values around −1.10 V vs. Ag/AgCl to −0.85 V vs. Ag/AgCl. A decrease in the onset potential for H_2 evolution implies an improvement on the reaction thermodynamics, since a lower overpotential was needed to produce H_2. Such an improvement suggests the settlement of a biofilm catalysing H_2 formation (Batlle-Vilanova et al., 2014; Perona-Vico et al., 2020).

However, an increase of current density was also detected between −0.3 and −0.7 V vs. Ag/AgCl, which could suggest some oxygen recycling on the cathode. It was assumed that the anode solely performed water oxidation into O_2. Evidences of hypochlorite formation were not detected due to the low chloride content (about 0.25 $gCl{\cdot}L^{-1}$, while saltwater is about 19 $gCl{\cdot}L^{-1}$) and the low current input (<0.4 $mA{\cdot}cm^{-2}$). Thus, O_2 reduction on the cathode suggested an accumulation of O_2 in the system. The presence of an excess of oxygen is not unexpected since HOBs require an H_2:O_2 ratio of 4:1 (Eq. 1, (Yu and Lu, 2019)), while water electrolysis is ideally producing H_2:O_2 at 2:1. For every mole of HOB produced (Eq. 1), 4 mol of H_2 and 1 mol of O_2 are consumed, while 1 mol of O_2 remains in excess. Gas composition analyses indicated that hydrogen gas was rarely detected in the headspace and it was found below the explosivity limit of 4% when biomass was present. Reactor A showed a maximum H_2 content in the headspace of 1.2% (day 14th). Reactor B showed a variable H_2 content in the headspace between 4.4 and 8.9% between days 0 and 17th (at the low frame of explosivity risk of 4–75%), where no biomass growth was observed. When biomass started to grow, H_2 rapidly disappeared and the maximum content detected was 0.2% (day 55th). On the contrary, oxygen concentration in the headspace was found between 21 and 39%. Fast hydrogen consumption by bacteria together with surplus oxygen recycling on the cathode clearly reduces the risks associated to H_2:O_2 explosive mixtures while reducing the costs associated to air sparging. However, O_2 accumulation can reduce the efficiency of the process by promoting nitrification (ammonium accumulation efficiency is decreased) and generating parasitic currents on the cathode (energy dissipation). A preliminary evaluation about the extent of oxygen recycling could be made by calculating a hydrogen yield for biomass based on the hypothesis that all current density was used to produce H_2. Under these circumstances, and taking the whole duration of the experiment (bulk liquid and biofilm biomass), a biomass hydrogen yield of 0.29 and 0.31 $gTSS{\cdot}gH_2^{-1}$ was observed for reactors A and B, respectively (Table 1). These values were lower than those presented in the literature for HOBs cultivated with sparged H_2 gas (1.04–2.32 $gTSS{\cdot}gH_2^{-1}$) (Garcia-Garcia et al., 2020; Matassa et al., 2016) or the stoichiometric values for *Cupriavidis necator* (1.52 $gTSS{\cdot}gH_2^{-1}$) (Yu and Lu, 2019). A similar difference can be observed with an immersed electrolyser with continuous CO_2:N_2 flushing (i.e. excess O_2 purged) if the hydrogen yield is estimated considering that all current supplied was

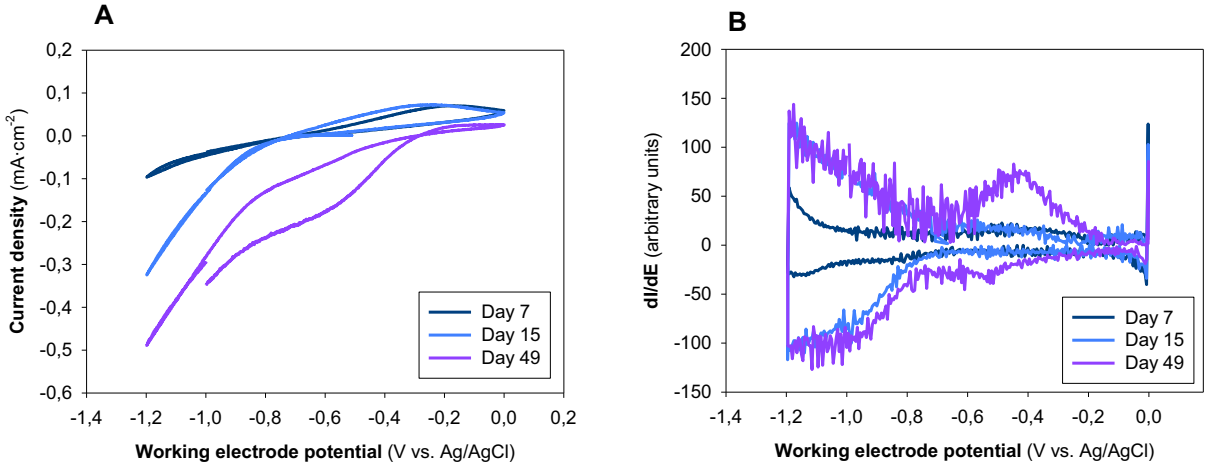

Fig. 2. Cyclic voltammetries performed on the cathode of reactor B: A) Current density response to working electrode potential. B) First derivatives of CVs. Only 3rd scans are shown.

dedicated to H_2 production (0.5–1.9 $gTSS{\cdot}gH_2^{-1}$) (Nyyssölä et al., 2021).

The relatively low hydrogen yields further supports the hypothesis that a fraction of the current density was dedicated to oxygen recycling on the cathode. An oxygen balance of the whole experiment can be performed by considering: i) the total amount of oxygen produced at the anode (144 ± 1 $mmoleO_2$), ii) the estimated magnitude of the nitrification process (9.8 ± 1.6 $mmoleO_2$), iii) the stoichiometric requirements for HOBs (7.1 ± 0.4 $mmoleO_2$) and iv) the oxygen detected (i.e. not consumed) (25.9 ± 9.5 $mmoleO_2$). The oxygen balance can estimate that about 102 ± 9 $mmoleO_2$ could have been reduced on the cathode surface (Fig. 3), accounting for 70 ± 6% of the current supplied to the system. The previous mass balance allows recalculating a hydrogen-to-biomass yield of 1.0 ± 0.1 $gTSS{\cdot}gH_2^{-1}$, which is in agreement with the values commonly found for HOBs (Christiaens et al., 2017; Matassa et al., 2016; Nyyssölä et al., 2021; Yu and Lu, 2019).

The energetic requirement dedicated to oxygen recycling had a direct impact on the energy efficiency of the system. An energetic efficiency of 3.7 and 3.0 $gTSS{\cdot}kWh^{-1}$ was observed in reactors A and B, respectively. Considering the stoichiometric hydrogen yield of an HOB (*Cupriavidis necator* - 1.52 $gTSS{\cdot}gH_2^{-1}$) (Yu and Lu, 2019), and the energetic requirements for existing H_2-producing technologies (22.4–96.3 $Wh{\cdot}gH_2^{-1}$ for steam methane reforming and coal gasification, respectively) (Batlle-Vilanova et al., 2014), the energetic cost could be ideally found between 15.8 and 67.9 $gTSS{\cdot}kWh^{-1}$. Further studies are required to investigate strategies for mitigating oxygen recycling on the cathode.

3.3. Community analyses

Samples were taken at the end of the study to analyze the bacterial community present in both the bulk liquid and the cathode electrode surface (Table 2). The predominant phyla in the samples were *Proteobacteria* (66.54–53.81%), *Bacteroidota* (30.87–13.80%), and *Actinobacteria* (18.54–4.34%). Being *Burkholderiales* (38.77–3.27%), *Rhizobiales* (42–11.80%) and *Xanthomonadales* (21.53–1.47%) the most represented orders.

Sequences belonging to the potentially HOB, such as *Hydrogenophaga flava*, *Xanthobacter flavus*, *Pelomonas* and *Rhizobium*, were among the most frequently found (7.6–26.5% in reactor A and 29.9–34.4% in reactor B). These percentages reveal a high level of diversity in the reactors, which is in concordance with the high diversity found when cultivating HOBs under batch conditions (Matassa et al., 2016). The same authors showed how the relative abundance of HOBs increased, resulting in better performances in terms of growth rates and yields, when they operated the system under continuous-flow mode. This suggests that a higher selective pressure to increase the abundance of HOBs could be obtained with the system operated under continuous-flow mode.

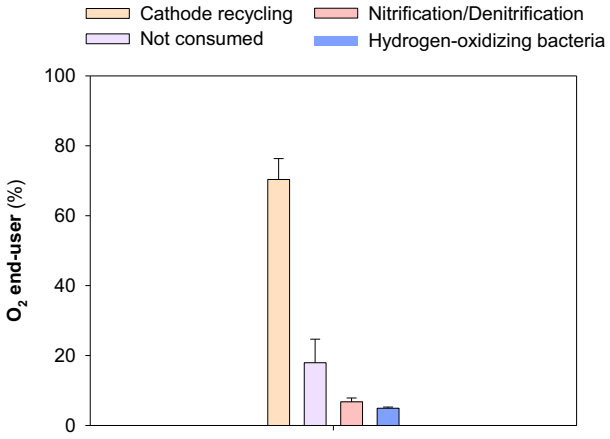

Fig. 3. Oxygen end-users in reactor replicates A and B presented as mean value ± standard deviation. Not consumed oxygen accounts for O_2 detected in the headspace and the liquid phase.

In reactor A, a nitrogen-fixing HOB, *Xanthobacter flavus* (Malik and Claus, 1979), was preferentially found on the cathode electrode (22.21%). In reactor B, *H. flava* was the dominant HOB either in the bulk liquid (18.7%) and the cathode electrode (21.92%). Both have been previously found in MET biocathodes for volatile fatty acids, CH_4 or H_2 production (Jourdin et al., 2016; Van Eerten-Jansen et al., 2013) and *Hydrogenophaga* are a known PHA accumulators (Crognale et al., 2019).

The combination of oxygen and ammonium in the same chamber also lead to the development of nitrifiers/denitrifiers such as *Stenotrophomonas nitritireducens* (Finkmann et al., 2000), *Devosia humi* (Ren et al., 2020), *Terrimonas suqianensis* (Liu et al., 2020) or *Niabella yanshanensis* (Bucci et al., 2020). Nitrifiers/denitrifiers accounted for 26.5–41.2% of abundance in reactor A, but less prominent in reactor B (12.7–15.0%). These results are in accordance with estimated nitrogen balance (Section 3.1.), which suggested that nitrification/denitrification could account for up to 56 and 44% of the nitrogen fate in reactors A and B, respectively. It might imply a competition with HOBs for ammonium but also for hydrogen, which could be used by hydrogenotrophic denitrifies. However, it has to be taken into account that some HOBs such as *Xanthobacter* also grow on nitrate (Murrell and Lidstrom, 1983).

Few differences were observed between the abundances found in the bulk liquid and the cathode electrode. The most relevant was *Mycolicibacterium insubricum*, which has been found in oxygen-reducing biocathodes (Zhang et al., 2017), which could contribute on mitigating the O_2:H_2 misbalance.

The presence of other members of the microbial community could help clarifying better the bio-reactor performance and potential. For example, the presence of polyhydroxyalkanoates accumulating *Sphingopyxis terrae* (Lam et al., 2017), which could increase the PHA production potential of the system together with the abilities of *Hydrogenophaga* (Crognale et al., 2019).

3.4. Potentialities and hurdles of electro-protein cultivation

The introduction of electrodes inside an HOB bioreactor can reduce the need of equipment for hydrogen production and storage, while reducing the risks associated to the formation of potentially explosive hydrogen mixtures. The concept of an electricity-driven MP production allows a tunable and apparently simple method to accumulate ammonium in form of a protein-rich biomass. Biomass was cultivated either in the bulk liquid or as biofilm (Fig. 4). Biomass cultivation on the electrode ensures a faster H_2 uptake and also enables a better biomass harvesting and dewatering, which could reduce the cost associated to biomass downstream processing. The maximum current density observed was low (<0.4 $mA{\cdot}cm^{-2}$), but this current input could be increased by further lowering of the cathode potential or by switching the operational mode to galvanostatic conditions.

The energetic costs observed for biomass growth in this study (3.3 ± 0.5 $gTSS{\cdot}kWh^{-1}$) were found to be higher than those expected by coupling hydrogen production in a MET (Batlle-Vilanova et al., 2014), with the cultivation of a pure HOB culture (*Cupriavidis necator*, 33 $gTSS{\cdot}kWh^{-1}$) (Yu and Lu, 2019). Results obtained suggested the presence of oxygen recycling on the cathode electrode together with the unwanted growth of nitrifying/denitrifying bacteria. Different alternatives to mitigate this issue could be explored such as regular oxygen wash-out by CO_2 sparging or the usage of 2-chambers MET, which is the most commonly used configuration for microbial electrosynthesis (Dessì et al., 2021). In addition, the promotion of bacterial growth directly from the electrode instead of H_2 mediation could also reduce the energetic demand of the system. In this latter case, either an anode for microbial H_2 oxidation (Hirose et al., 2021) or a cathode for O_2 reduction (Hoareau et al., 2021) could be alternatives to be explored because of the high protein conversion efficiency of microorganisms in respect to

Table 2
Most abundant ASVs after comparison of sequences with the NCBI GenBank database.

Number ASVs	Most probable identification (% similarity)	Sequence similarity range (%)	Relative abundance (% of sequences)			
			Reactor A		Reactor B	
			Bulk liquid	Cathode electrode	Bulk liquid	Cathode electrode
Proteobacteria						
ASV1	(NR_114133.1) *Hydrogenophaga flava* strain NBRC 102514	100	0.56	2.41	18.7	21.92
ASV4	(NR_113665.1) *Xanthobacter flavus* strain NBRC 14759	100	3.65	22.21	1.43	1.59
ASV2	(NR_025305.1) *Stenotrophomonas nitritireducens* strain L2	100	20.98	15.23	0.51	0.62
ASV3	(NR_113727.1) *Sphingopyxis terrae* strain NBRC 15098	99.6	12.88	5.38	5.46	2.79
ASV6	(NR_114189.1) *Pelomonas saccharophila* strain NBRC 103037	100	2.9	0.56	7.08	6.83
ASV8	(NR_115018.1) *Pararhodobacter aggregans* strain D1–19	98.81	ND	ND	3.45	6.99
ASV11	(NR_117715.1) *Afipia felis* strain CIP 103515	100	3.00	4.33	3.73	2.51
ASV14	(NR_147759.1) *Devosia humi* strain THG-MM1	100	2.76	4.01	2.86	2.79
ASV15	(NR_118139.1) *Rhizobium mesoamericanum* CCGE 501	100	0.48	1.35	2.73	4.01
ASV26	(NR_134182.1) *Sphingomonas kyeonggiensis* strain THG-DT81	100	3.26	0.34	0.14	ND
Bacteroidota						
ASV10	(NR_164880.1) *Terrimonas suqianensis* strain C3–5	100	12.71	5.33	4.95	3.97
ASV5	(NR_116677.1) *Niabella yanshanensis* strain CCBAU 05354	98.42	4.71	1.93	6.63	5.31
ASV16	(NR_134729.1) *Flavobacterium qiangtangense* strain F3	96.05	5.99	3.35	0.61	0.35
Actinobacteria						
ASV7	(NR_125525.1) *Mycolicibacterium insubricum* strain FI-06250	100	4.08	17.98	9.65	15.21

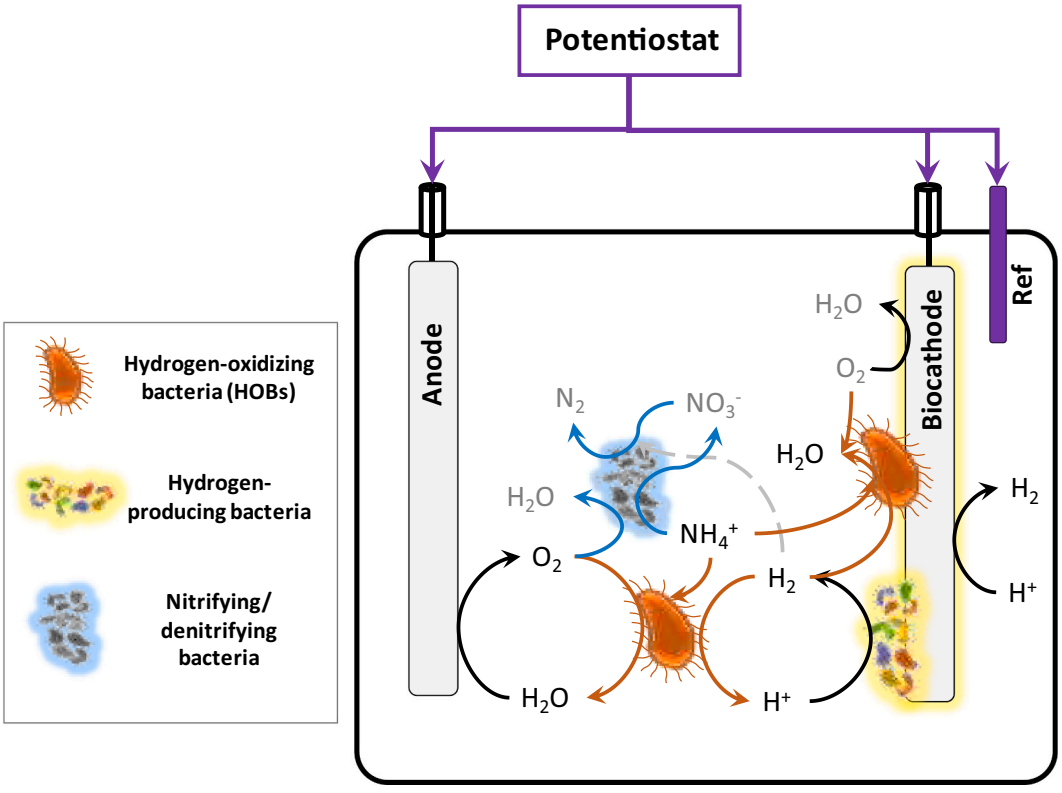

Fig. 4. Set of wanted and unwanted reactions occurring in the electro-protein set-up.

animal- or plant-based farming systems (Galloway and Cowling, 2002; Matassa et al., 2015a; Pikaar et al., 2017).

4. Conclusions

This work explored the use of MET for electricity-driven ammonium accumulation into biomass (protein content between 53 ± 8 and 64 ± 4%). Mixed-culture biomass was cultivated (*Hydrogenophaga*, *Xanthobacter* as the main HOBs). Immersion of electrodes in the bioreactor allowed to safely provide in-situ oxygen and hydrogen. For an increase of 0.1 $mA{\cdot}cm^{-2}$, the suspended biomass increased 101–124 $mgTSS{\cdot}L^{-1}$. Biomass growth occurred both in the bulk liquid and on the cathode electrode surface, offering an alternative strategy for MP harvesting. However, electro-microbial cultivation requires further improvements to reduce oxygen recycling and achieve higher volumetric biomass productivities.

CRediT authorship contribution statement

Narcís Pous: Conceptualization, Data curation, Investigation, Methodology, Writing – original draft. **M. Dolors Balaguer:** Conceptualization, Funding acquisition, Methodology, Supervision, Writing – review & editing. **Silvio Matassa:** Data curation, Writing – review & editing. **Paola Chiluiza-Ramos:** Data curation, Investigation, Writing – review & editing. **Lluis Bañeras:** Conceptualization, Funding acquisition, Methodology, Supervision, Investigation, Writing – review & editing. **Sebastià Puig:** Conceptualization, Funding acquisition, Methodology, Supervision, Project administration, Writing – review & editing.

Declaration of competing interest

The authors declare that they have no known competing financial interests or personal relationships that could have appeared to influence the work reported in this paper.

Acknowledgements

This research was carried out in the project “RITA – urban cycle ResIlient To pAndemics) funded by AGAUR (ref. 2020PANDE00176). The authors acknowledge the technical support of Ms. Sandra Cano and Mr. Juan José Murga. S.P. is a Serra Hunter Fellow (UdG-AG-575) and acknowledges the funding from the ICREA Academia award. LEQUIA (2017-SGR-1552) and Ecoaqua (2017-SGR-548) have been recognized as consolidated research groups by the Catalan Government.

Appendix A. Supplementary data

Supplementary data to this article can be found online at https://doi.org/10.1016/j.biteb.2022.101010.

References

APHA, 2005. Standard Methods for the Examination of Water and Wastewater, 19th ed. Washington DC, USA.

Batlle-Vilanova, P., Puig, S., Gonzalez-Olmos, R., Vilajeliu-Pons, A., Bañeras, L., Balaguer, M.D., Colprim, J., 2014. Assessment of biotic and abiotic graphite cathodes for hydrogen production in microbial electrolysis cells. Int. J. Hydrog. Energy 39, 1297–1305. https://doi.org/10.1016/j.ijhydene.2013.11.017.

Bucci, P., Coppotelli, B., Morelli, I., Zaritzky, N., Caravelli, A., 2020. Simultaneous heterotrophic nitrification and aerobic denitrification of wastewater in granular reactor: Microbial composition by next generation sequencing analysis. J. Water Process Eng. 36 https://doi.org/10.1016/j.jwpe.2020.101254.

Callahan, B.J., McMurdie, P.J., Rosen, M.J., Han, A.W., Johnson, A.J.A., Holmes, S.P., 2016. DADA2: High-resolution sample inference from Illumina amplicon data. Nat. Methods 13, 581–583. https://doi.org/10.1038/nmeth.3869.

Christiaens, M.E.R., Gildemyn, S., Matassa, S., Ysebaert, T., De Vrieze, J., Rabaey, K., 2017. Electrochemical ammonia recovery from source-separated urine for microbial protein production. Environ. Sci. Technol. 51, 13143–13150. https://doi.org/10.1021/acs.est.7b02819.

Crognale, S., Tonanzi, B., Valentino, F., Majone, M., Rossetti, S., 2019. Microbiome dynamics and phaC synthase genes selected in a pilot plant producing polyhydroxyalkanoate from the organic fraction of urban waste. Sci. Total Environ. 689, 765–773. https://doi.org/10.1016/j.scitotenv.2019.06.491.

De Vrieze, J., Verbeeck, K., Pikaar, I., Boere, J., Van Wijk, A., Rabaey, K., Verstraete, W., 2020. The hydrogen gas bio-based economy and the production of renewable building block chemicals, food and energy. New Biotechnol. 55, 12–18. https://doi.org/10.1016/j.nbt.2019.09.004.

Dessì, P., Rovira-Alsina, L., Sánchez, C., Dinesh, G.K., Tong, W., Chatterjee, P., Tedesco, M., Farràs, P., Hamelers, H.M.V., Puig, S., 2021. Microbial electrosynthesis: Towards sustainable biorefineries for production of green chemicals from CO2 emissions. Biotechnol. Adv. 46 https://doi.org/10.1016/j.biotechadv.2020.107675.

Dou, J., Huang, Y., Ren, H., Li, Z., Cao, Q., Liu, X., Li, D., 2019. Autotrophic, heterotrophic, and mixotrophic nitrogen assimilation for single-cell protein production by two hydrogen-oxidizing bacterial strains. Appl. Biochem. Biotechnol. 187, 338–351. https://doi.org/10.1007/s12010-018-2824-1.

EU Hydrogen Strategy, 2020. EU Hydrogen Strategy [WWW Document]. EU Hydrog. Strateg. Factsheet. https://ec.europa.eu/commission/presscorner/detail/en/FS_20_1296.

Finkmann, W., Altendorf, K., Stackebrandt, E., Lipski, A., 2000. Characterization of N2O-producing Xanthomonas-like isolates from biofilters as Stenotrophomonas nitritireducens sp. nov., Luteimonas mephitis gen. nov., sp. nov. And Pseudoxanthomonas broegbernensis gen. nov., sp. nov. Int. J. Syst. Evol. Microbiol. 50, 273–282. https://doi.org/10.1099/00207713-50-1-273.

Galloway, J.N., Cowling, E.B., 2002. Reactive nitrogen and the world: 200 years of change. Ambio 31, 64–71. https://doi.org/10.1579/0044-7447-31.2.64.

Garcia-Garcia, G., Fernandez, M.C., Armstrong, K., Woolass, S., Styring, P., 2020. Analytical review of life-cycle environmental impacts of carbon capture and utilization technologies. ChemSusChem 995–1015. https://doi.org/10.1002/cssc.202002126.

Givirovskiy, G., Ruuskanen, V., Ojala, L.S., Kokkonen, P., Ahola, J., 2019. In situ water electrolyzer stack for an electrobioreactor. Energies 12. https://doi.org/10.3390/en12101904.

Hirose, A., Kouzuma, A., Watanabe, K., 2021. Hydrogen-dependent current generation and energy conservation by Shewanella oneidensis MR-1 in bioelectrochemical systems. J. Biosci. Bioeng. 131, 27–32. https://doi.org/10.1016/j.jbiosc.2020.08.012.

Hoareau, M., Erable, B., Bergel, A., 2021. Oxygen-reducing bidirectional microbial electrodes: a mini-review. Electrochem. Commun. 123 https://doi.org/10.1016/j.elecom.2021.106930.

Holladay, J.D., Hu, J., King, D.L., Wang, Y., 2009. An overview of hydrogen production technologies. Catal. Today 139, 244–260. https://doi.org/10.1016/j.cattod.2008.08.039.

Hosseini, S.E., Wahid, M.A., 2016. Hydrogen production from renewable and sustainable energy resources: promising green energy carrier for clean development. Renew. Sustain. Energ. Rev. 57, 850–866. https://doi.org/10.1016/j.rser.2015.12.112.

Jourdin, L., Lu, Y., Flexer, V., Keller, J., Freguia, S., 2016. Biologically Induced Hydrogen Production Drives High Rate/High Efficiency Microbial Electrosynthesis of Acetate from Carbon Dioxide. ChemElectroChem 3, 581–591. https://doi.org/10.1002/celc.201500530.

Kozich, J.J., Westcott, S.L., Baxter, N.T., Highlander, S.K., Schloss, P.D., 2013. Development of a dual-index sequencing strategy and curation pipeline for analyzing amplicon sequence data on the MiSeq Illumina sequencing platform. Appl. Environ. Microbiol. 79, 5112–5120.

Kundu, A., Sahu, J.N., Redzwan, G., Hashim, M.A., 2013. An overview of cathode material and catalysts suitable for generating hydrogen in microbial electrolysis cell. Int. J. Hydrog. Energy 38, 1745–1757. https://doi.org/10.1016/j.ijhydene.2012.11.031.

Lai, A., Aulenta, F., Mingazzini, M., Palumbo, M.T., Papini, M.P., Verdini, R., Majone, M., 2017. Bioelectrochemical approach for reductive and oxidative dechlorination of chlorinated aliphatic hydrocarbons (CAHs). Chemosphere 169, 351–360. https://doi.org/10.1016/j.chemosphere.2016.11.072.

Lam, W., Wang, Y., Chan, P.L., Chan, S.W., Tsang, Y.F., Chua, H., Yu, P.H.F., 2017. Production of polyhydroxyalkanoates (PHA) using sludge from different wastewater treatment processes and the potential for medical and pharmaceutical applications. Environ. Technol. (U. K.) 38, 1779–1791. https://doi.org/10.1080/09593330.2017.1316316.

Liu, C., Colón, B.C., Ziesack, M., Silver, P.A., Nocera, D.G., 2016. Water splitting-biosynthetic system with CO2 reduction efficiencies exceeding photosynthesis. Science (80-.) 352, 1210–1213. https://doi.org/10.1126/science.aaf5039.

Liu, T., He, X., Jia, G., Xu, J., Quan, X., You, S., 2020. Simultaneous nitrification and denitrification process using novel surface-modified suspended carriers for the treatment of real domestic wastewater. Chemosphere 247. https://doi.org/10.1016/j.chemosphere.2020.125831.

Malik, K.A., Claus, D., 1979. Xanthobacter flavus, a new species of nitrogen-fixing hydrogen bacteria. Int. J. Syst. Bacteriol. 29, 283–287. https://doi.org/10.1099/00207713-29-4-283.

Matassa, S., Batstone, D.J., Hülsen, T., Schnoor, J., Verstraete, W., 2015a. Can direct conversion of used nitrogen to new feed and protein help feed the world? Environ. Sci. Technol. 49, 5247–5254. https://doi.org/10.1021/es505432w.

Matassa, S., Boon, N., Verstraete, W., 2015b. Resource recovery from used water: the manufacturing abilities of hydrogen-oxidizing bacteria. Water Res. 68, 467–478. https://doi.org/10.1016/j.watres.2014.10.028.

Matassa, S., Verstraete, W., Pikaar, I., Boon, N., 2016. Autotrophic nitrogen assimilation and carbon capture for microbial protein production by a novel enrichment of

hydrogen-oxidizing bacteria. Water Res. 101, 137–146. https://doi.org/10.1016/j.watres.2016.05.077.

Matassa, S., Papirio, S., Pikaar, I., Hülsen, T., Leijenhorst, E., Esposito, G., Pirozzi, F., Verstraete, W., 2020. Upcycling of biowaste carbon and nutrients in line with consumer confidence: the "full gas" route to single cell protein. Green Chem. 22, 4912–4929. https://doi.org/10.1039/D0GC01382J.

Murrell, J.C., Lidstrom, M.E., 1983. Nitrogen metabolism in Xanthobacter H4–14. Arch. Microbiol. 136, 219–221. https://doi.org/10.1007/BF00409848.

Nyyssölä, A., Ojala, L.S., Wuokko, M., Peddinti, G., Tamminen, A., Tsitko, I., Nordlund, E., Lienemann, M., 2021. Production of Endotoxin-free Microbial Biomass for Food Applications by Gas Fermentation of Gram-positive H2-oxidizing Autotrophic Bacteria. https://doi.org/10.1021/acsfoodscitech.0c00129. Submitted for publication.

Perona-Vico, E., Feliu-Paradeda, L., Puig, S., Bañeras, L., 2020. Bacteria coated cathodes as an in-situ hydrogen evolving platform for microbial electrosynthesis. Sci. Rep. 10, 19852. https://doi.org/10.1038/s41598-020-76694-y.

Pikaar, I., Matassa, S., Rabaey, K., Bodirsky, B.L., Popp, A., Herrero, M., Verstraete, W., 2017. Microbes and the next nitrogen revolution. Environ. Sci. Technol. 51, 7297–7303. https://doi.org/10.1021/acs.est.7b00916.

Pous, N., Puig, S., Balaguer, M.D., Colprim, J., 2017. Effect of hydraulic retention time and substrate availability in denitrifying bioelectrochemical systems. Environ. Sci. Water Res. Technol. 3 https://doi.org/10.1039/c7ew00145b.

Rabaey, K., Ossieur, W., Verhaege, M., Verstraete, W., 2005. Continuous microbial fuel cells convert carbohydrates to electricity. Water Sci. Technol. 52, 515–523.

Ren, Y., Lv, Y., Wang, Y., Li, X., 2020. Effect of heterotrophic anodic denitrification on anolyte pH control and bioelectricity generation enhancement of bufferless microbial fuel cells. Chemosphere 257. https://doi.org/10.1016/j.chemosphere.2020.127251.

Rovira-Alsina, L., Perona-Vico, E., Bañeras, L., Colprim, J., Balaguer, M.D., Puig, S., 2020. Thermophilic bio-electro CO2 recycling into organic compounds. Green Chem. 22, 2947–2955. https://doi.org/10.1039/d0gc00320d.

Rozendal, R.A., Jeremiasse, A.W., Hamelers, H.V.M., Buisman, C.J.N., 2008. Hydrogen production with a microbial biocathode. Environ. Sci. Technol. 42, 629–634. https://doi.org/10.1021/es071720+.

Ruuskanen, V., Givirovskiy, G., Elfving, J., Kokkonen, P., Karvinen, A., Järvinen, L., Sillman, J., Vainikka, M., Ahola, J., 2021. Neo-carbon food concept: a pilot-scale hybrid biological–inorganic system with direct air capture of carbon dioxide. J. Clean. Prod. 278 https://doi.org/10.1016/j.jclepro.2020.123423.

Sillman, J., Nygren, L., Kahiluoto, H., Ruuskanen, V., Tamminen, A., Bajamundi, C., Nappa, M., Wuokko, M., Lindh, T., Vainikka, P., Pitkänen, J.P., Ahola, J., 2019. Bacterial protein for food and feed generated via renewable energy and direct air capture of CO2: can it reduce land and water use? Glob. Food Sec. 22, 25–32. https://doi.org/10.1016/j.gfs.2019.09.007.

Van Eerten-Jansen, M.C.A.A., Veldhoen, A.B., Plugge, C.M., Stams, A.J.M., Buisman, C.J.N., Ter Heijne, A., 2013. Microbial community analysis of a methane-producing biocathode in a bioelectrochemical system. Archaea 2013. https://doi.org/10.1155/2013/481784.

Vilajeliu-Pons, A., Bañeras, L., Puig, S., Molognoni, D., Vilà-Rovira, A., Amo, E.H.Del, Balaguer, M.D., Colprim, J., 2016. External resistances applied to MFC affect core microbiome and swine manure treatment efficiencies. PLoS One 11, 1–19. https://doi.org/10.1371/journal.pone.0164044.

Volova, T.G., Barashkov, V.A., 2010. Characteristics of proteins synthesized by hydrogen-oxidizing microorganisms. Appl. Biochem. Microbiol. 46, 574–579. https://doi.org/10.1134/S0003683810060037.

Yu, J., Lu, Y., 2019. Carbon dioxide fixation by a hydrogen-oxidizing bacterium: biomass yield, reversal respiratory quotient, stoichiometric equations and bioenergetics. Biochem. Eng. J. 152, 107369 https://doi.org/10.1016/j.bej.2019.107369.

Zhang, G., Feng, S., Jiao, Y., Lee, D.-J., Xin, Y., Sun, H., 2017. Cathodic reducing bacteria of dual-chambered microbial fuel cell. Int. J. Hydrog. Energy 42, 27607–27617. https://doi.org/10.1016/j.ijhydene.2017.06.095.

Zhang, W., Zhang, F., Niu, Y., Li, Y.-X., Jiang, Y., Bai, Y.-N., Dai, K., Zeng, R.J., 2020. Power to hydrogen-oxidizing bacteria: effect of current density on bacterial activity and community spectra. J. Clean. Prod. 263 https://doi.org/10.1016/j.jclepro.2020.121596.